A COHESIVE ZONE MODEL FOR STUDYING CRACK GROWTH IN MATERIALS AND STRUCTURES

HAODAN JIANG, XIAOSHENG GAO AND **T. S. SRIVATSAN**
Department of Mechanical Engineering
The University of Akron
Akron, Ohio 44325
xgao@uakron.edu, tss1@uakron.edu

Abstract: This paper presents a cohesive zone model and explores its capacity for predicting crack growth in materials and structures. An exponential cohesive law was implemented for the specific case of monotonic loading and applied to crack growth simulation, in three-dimensions, in thin fracture specimens made from the chosen material of interest. The cohesive law is governed by the two parameters, cohesive strength and cohesive energy, and our parameter study revealed the cohesive strength to be a more influential parameter. The cohesive parameters were calibrated for the commercial aluminum-copper-magnesium alloy 2024 in the T3 temper by comparing the finite element predictions with experimental test results obtained for a compact-tension specimen. Middle-cracked tension test specimens having different ratios of the crack length were modeled using the calibrated parameters and the numerical results showed good correlation with the experimental test results.

1.   INTRODUCTION

Failure of engineering structures can occur from either one or a combination of reasons. Often in practice disasters tend to occur primarily because the relevant engineering structure contains cracks, which occur and exist either during production or during service. The consequences of failure can often be catastrophic. Over the last four decades, several contributions have been made towards enriching our prevailing understanding of crack-related structural failures and as a direct consequence various approaches have been introduced.

The science of fracture mechanics provides different concepts of a single parameter for the purpose of evaluating crack growth through a test specimen or structure. The stress intensity factor (SIF) (Irwin, 1956) [10], referred to henceforth through this manuscript as K, has proven to be a useful tool for both studying and understanding problems related to the fracture of solids having pre-existing flaws and a negligible non-linear zone ahead of the crack tip. Yet, it is understood that the stress intensity factor is limited to conditions where essentially linear-elasticity prevails in the cracked body, such as small scale yielding. The concept of Elastic-Plastic Fracture Mechanics, referred to henceforth as EPFM, was developed for studying ductile fracture of solids that experience a substantial amount of plastic deformation. The path-independent contour integral *J*-integral, put forth by James Rice (Rice, 1968) [25], is usually used in rate-independent quasi-static fracture analysis with the primary objective of characterizing the energy release during crack growth. However, the assumption of non-linear elasticity, or deformation

---

theory of plasticity, applies only to monotonic loading of elastic-plastic materials. Another noticeable limitation is the use of small deformation theory to prove the path-independence of the J-integral.

The concept of cohesive zone was initially conceived by Dugdale in 1960 [7], Barenblatt in 1962 [2], Rice in 1968 [25] and a few others during the subsequent years. This concept regards fracture to be a gradual phenomenon in which separation occurs between two adjacent virtual surfaces across an extended crack tip (cohesive zone) and is often resisted by the presence of cohesive forces. This theory of fracture led to a novel numerical approach to simulate and study crack propagation. In this approach, the continuum is characterized by two constitutive relations:

(i)   A volumetric constitutive model describing the "bulk behavior" of the material.
(ii)   A cohesive surface constitutive relation between the traction and displacement characterizing the behavior of bond surfaces between the elements.

Over the years, the Cohesive Zone Model (referred to as CZM) has been successfully applied for studying and rationalizing crack growth simulation in materials spanning the domains of metals, concretes, ceramics, polymers, and even their composite counterparts, i.e., metal-matrix composites (MMCs), ceramic-matrix composites (CMCs) and polymer-matrix composites (PMCs). Examples include the following: (a) quasi-static fracture simulations (Roy and Dodds, 2002 [27], (b) dynamic crack growth (Xu and Needleman, 1994 [35], Siegmund and Needleman, 1997 [30]), (c) fragmentation (Camacho and Ortiz, 1996 [4]; Miller, Freund and Needleman, 1999 [18], Zhai and Zhou, 1999 [36], Repetto, Radovitzky and Ortiz, 2000 [24]), (d) creep behavior (Bouvard, Chabocheb, 2009 [3]), and (e) separation stability (Suo, Ortiz, Needleman, 1992 [32]; Levy, 1994 [15]).

The specific study becomes complex for three-dimensional applications due to complexity of the local stress state coupled with crack branching/tunneling. Lin and Cornec, 1998 [17] simulated 3-D crack extension using the cohesive zone model for: (a) side-grooved compact tension specimen, and (b) a surface-crack tension specimen. Their results presented good agreement with the experimental findings. Subsequently, Ortiz, Pandolfi, 1999 [21] and Pandolfi and Guduru, 2000 [22] employed a similar type of triangular cohesive element to simulate 3-D dynamic crack extension in solids that undergo large scale plasticity. This led Foulk and coworkers, 2000 [9] to apply 3-D cohesive zone models for the purpose of studying crack growth in brittle composites. The success achieved by the earlier researchers motivated Roy and Dodds, 2001 [26] to study ductile crack extension in thin aluminum panels under the influence of quasi-static loading using the cohesive zone model. The specific aspect of crack path deviation during stable crack extension in ductile materials was investigated by Scheider, 2001 [28], Scheider and Brocks, 2003 [29] by placing interface elements between all the continuum elements and successfully captured the phenomenon of cup–cone fracture of a round tensile bar of a ductile solid subjected to monotonic loading.

This paper presents the results of a study on crack growth under monotonic loading using a 3-D exponential cohesive zone model. The constitutive behavior between the crack surfaces was formulated considering: (i) local unloading and reloading, and (ii) potential contact phenomenon. The quasi-static fracture analysis was performed on a thin sheet Compact Tension (CT) specimen and the three-dimensional cohesive zone model and resultant cohesive parameters were calibrated by fitting with results obtained from experiments. Middle-crack Tension (MT) specimens made of the same sheet material were then modeled using the cohesive zone model with the calibrated parameters by considering the effect of the ratio of the initial crack length to specimen width.

2.   FORMULATION OF THE COHESIVE ZONE MODEL

Consider a quasi-static solid specimen having cracked surfaces. Along the potential crack path a pair of virtual crack surfaces is assumed, which is subjected to a separating force that is referred to as cohesive traction. Based on the principle of virtual work, the equation for mechanical equilibrium considering the contribution of the cohesive tractions can be expressed as

$$\int_V \vec{s} : \delta \vec{F} dV - \int_{S_{\text{int}}} \vec{T}_{CZ} \cdot \delta \vec{\Delta} dS = \int_{S_{ext}} \vec{T}_{ext} \cdot \delta \vec{u} dS \qquad (1)$$

where in this expression:
(a) V is the specimen volume, S_{int} the internal (cohesive) surface, and S_{ext} represents the external surface.

(b) $\vec{s}$ is the nominal stress tensor $s = F^{-1} \det(F) \sigma$, where $\vec{F}$ is the deformation gradient and σ is the Cauchy stress;

(c) $\vec{T}_{CZ}$ denotes the cohesive traction vector while $\vec{T}_{ext}$ is the external traction vector.

(d) $\vec{u}$ is the displacement vector and $\vec{\Delta} = u^+ - u^-$ represents the displacement jump across two adjacent cohesive surfaces.

(e) $\vec{\Delta}$ is referred to as the relative displacement vector, or the separation vector.

The cohesive surface contributions are well described by an integration term over the internal surface $\int_{S_{\text{int}}} \vec{T}_{CZ} \cdot \delta \vec{\Delta} dS$. Comparable to the deformation behavior of the bulk material that can be easily described with conventional stress-strain relationships; the evolution of separation that occurs due to local traction at the crack tip can be defined using a constitutive law for a special field between the virtual crack surfaces. The cohesive traction and separation are work conjugate, just as stress and strain being strain energy conjugate.

For isothermal conditions, based on the First and Second laws of thermodynamics, the traction vector acting on the cohesive surfaces ($\vec{T}_{CZ}$), simplified as $\vec{T}$ henceforth through this manuscript, can be derived using the interfacial potential $\phi(\vec{\Delta})$ (Needleman, 1992 [19])

$$\vec{T} = \frac{\partial \phi(\vec{\Delta})}{\partial \vec{\Delta}} \qquad (2)$$

$\phi(\vec{\Delta})$ represents the free energy density function per unit undeformed area. By selecting   a proper potential function (ϕ), the constitutive equation between the cohesive traction and relative separation can be formulated. Under 3-D configuration, both $\vec{\Delta}$ and $\vec{T}$ have three components (normal, tangential and transverse). We adopt the following notation:
(i) $\vec{\Delta} = (\Delta u_n, \Delta u_{t1}, \Delta u_{t2})$, and

(ii) $\vec{T} = (T_n, T_{t1}, T_{t2})$,

where $\Delta u_n = \vec{\Delta} \cdot \vec{n}$; $\Delta u_{t1} = \vec{\Delta} \cdot \vec{t}_1$; $\Delta u_{t2} = \vec{\Delta} \cdot \vec{t}_2$; and $T_n = \vec{T} \cdot \vec{n}$; $T_{t1} = \vec{T} \cdot \vec{t}_1$; $T_{t2} = \vec{T} \cdot \vec{t}_2$.

Different potential forms, divided between linear/bilinear, polynomial and exponential forms, have been adopted by the researchers in their independent studies. The present study chooses the computationally convenient exponential form of the free energy density potential

$$\phi(\vec{\Delta}) = \sigma_{max,0} e \delta_0 (1.0 + \frac{\Delta u_n}{\delta_0}) \exp(-\frac{\Delta u_n}{\delta_0})[(1.0 - q) + q \exp(-\frac{\Delta u_{t1}^2 + \Delta u_{t2}^2}{\delta_0^2}))] \qquad (3)$$

where $\sigma_{max,0}$ is the initial normal cohesive strength under monotonic loading, δ_0 is the characteristic cohesive length, i.e. the material separation required to achieve the normal cohesive strength. q is the ratio between the normal cohesive energy Γ_n and shear cohesive energy Γ_t. The cohesive energy is the energy needed to fail the cohesive zone and to concurrently create a unit area of new free surface. With the assumption of transverse isotropy, the same shear cohesive energy for both the tangential and transverse directions are used: $\Gamma_{t1} = \Gamma_{t2} = \Gamma_t$ and $q = \Gamma_t / \Gamma_n$.

2.1 The cohesive traction-separation law for monotonic loading

In this section we consider the monotonic loading situation with no degradation in the cohesive strength to be accounted for. The cohesive traction components can be computed from derivatives of the potential function and are expressed as follows:

$$T_n = \frac{\partial \phi}{\partial \Delta u_n}, \quad T_{t1} = \frac{\partial \phi}{\partial \Delta u_{t1}}, \quad T_{t2} = \frac{\partial \phi}{\partial \Delta u_{t2}}$$

Taking into consideration the free energy density potential, we now have the separation law for cohesive traction for the case of monotonic loading

$$T_n = \sigma_{max,0} \Delta u \exp(1 - \Delta u)\{(1 - q) + q \exp(-\Delta v_1^2 - \Delta v_2^2)\} \qquad (4a)$$

$$T_{t1} = 2q\sigma_{max,0} (1 + \Delta u)\Delta v_1 \exp(1 - \Delta u) \exp(-\Delta v_1^2 - \Delta v_2^2) \qquad (4b)$$

$$T_{t2} = 2q\sigma_{max,0} (1 + \Delta u)\Delta v_2 \exp(1 - \Delta u) \exp(-\Delta v_1^2 - \Delta v_2^2) \qquad (4c)$$

where Δu, Δv_1 and Δv_2 are the normalized normal, tangential and transverse separation components respectively

$$\Delta u = \frac{\Delta u_n}{\delta_0} \qquad \Delta v_1 = \frac{\Delta u_{t1}}{\delta_0} \qquad \Delta v_2 = \frac{\Delta u_{t2}}{\delta_0}.$$

The features of the traction-separation constitutive equations defined for both the pure normal condition and pure shear condition are illustrated in the normalized form in Figure 1. The traction values are normalized with respect to the corresponding cohesive strength $\sigma_{max,0}$ (normal cohesive strength) or $\tau_{i max,0}$ (shear cohesive strength, $i = 1, 2$ for the tangential and transverse directions respectively), and the separation values are normalized with respect to the characteristic cohesive length (δ_0). As shown in Figure 1, the cohesive traction increases monotonically with increasing separation prior to the characteristic separation at which point the cohesive strength ($\sigma_{max,0}$ or $\tau_{i max,0}$) is achieved. For the case of pure normal loading the characteristic separation is δ_0, and for the case of pure shear (tangential and transverse) loading this separation value equals $\sqrt{2}\delta_0 / 2$. Subsequently, the traction value decreases with increasing separation and approaches to zero eventually.

The cohesive strength is taken to be the peak value of the cohesive traction. Further, it represents the maximum resistance offered by the material to crack opening under pure loading

modes ($\sigma_{\max,0}$ for normal and $\tau_{i\max,0}$ for shear). Assuming the existence of in-plane isotropy, the initial shear cohesive strength under conditions of pure shear can be defined from the constitutive laws as

$$\tau_{1\max,0} = \tau_{2\max,0} = \sqrt{2e}q\sigma_{\max,0}$$

In this expression q is the ratio of the shear cohesive energy (Γ_t) to the normal cohesive energy (Γ_n).

The cohesive energy, or work of separation, per unit area, of the cohesive surface, is defined as

$$\Gamma = \int_0^{\infty} Td\Delta \tag{5}$$

It is represented by the area enclosed under the traction-separation curve. With the exponential constitutive law given by Equation (3), the critical cohesive energy for: (a) pure normal loading, and for (b) pure shear loading are as follows:

$$\Gamma_n = e\sigma_{\max,0}\delta_0,$$

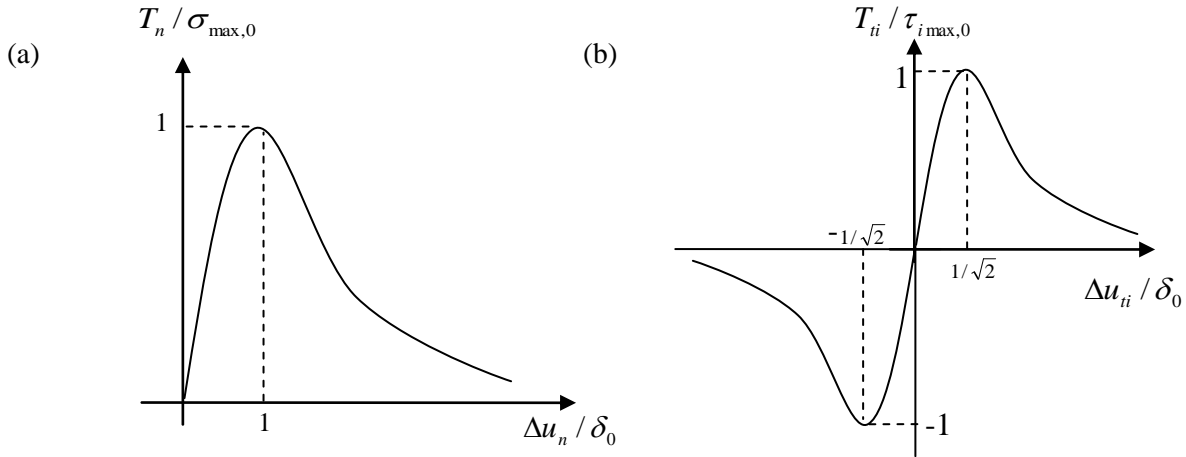$$\Gamma_{ti} = eq\sigma_{\max,0}\delta_0 = \sqrt{\frac{e}{2}}\tau_{i\max,0}\delta_0 \quad (i=1,2).$$

Figure 1. **Monotonic traction-separation relation under (a) pure normal, and (b) Pure shear (tangential: $i = 1$; transverse: $i = 2$) loading.**

2.2 Unloading/reloading

To account for the partial unloading and reloading, which occurs with crack propagation, the paths of unloading and reloading need to be well defined in the cohesive zone model. When separation of the cohesive surfaces becomes smaller than the previous loading state, the path of unloading is followed. In this research effort, unloading is prescribed to be directed back to the origin of the traction-separation space (Figure 2). The traction components during unloading are calculated as follows.

$$T_n = \Delta u_n * k_{n,0} \qquad T_{t1} = \Delta u_{t1} * k_{t1,0} \qquad T_{t2} = \Delta u_{t2} * k_{t2,0} \tag{6}$$

where in this expression

(i) $\quad k_{n,0} = T_{n,\max} / \Delta u_{n,\max}, \quad k_{t1,0} = T_{t1,\max} / \Delta u_{t1,\max}, \quad k_{t2,0} = T_{t2,\max} / \Delta u_{t2,\max} \qquad$ are the constant unloading stiffness;

(ii) $\Delta u_{n,\max}$, $\Delta u_{t1,\max}$ and $\Delta u_{t2,\max}$ are values of the separation components at the onset of unloading; and

(iii) $T_{n,\max}$, $T_{t1,\max}$ and $T_{t2,\max}$ are the corresponding traction values up until maximum separation.

When the current separation overpasses the previous value but is smaller than the maximum separation, the relation for traction separation follows a reloading path. For the case of monotonic loading with no damage accumulation, reloading takes place along the reverse direction of the unloading path before it meets with the loading curve (Figure 2). Under such circumstances, the reloading stiffness equals the unloading stiffness.

2.3 Compression/normal contact of broken cohesive surfaces

During unloading in the normal direction, the unloading path may reach $\Delta u_n = 0$, and the crack surfaces came into contact with each other. In order to avoid overlapping and interpenetration of the material surfaces, a penalty is taken for the cohesive traction corresponding to $\Delta u_n < 0$. The penalized equation for contact computation can be expressed as

$$T_n = A\sigma_{\max,0}\Delta u \exp(1 - \Delta u) \tag{7}$$

In this equation, the stiffness multiplier (A) penalizes any negative value of Δu thereby preventing the solid elements that surround the cohesive element from interpenetrating each other. However, the value of the penalty multiplier has to be appropriate such that negative separation can be resisted while it should not be too big to introduce effects due to adverse loading. In the present study, the value of A is chosen to be equal to 30 after trial and error adjustments.

It is worth noting that no other fracture criterion is necessary to complete the description of the Cohesive Zone Model. The opening of new crack surfaces is the natural result of an evolvement of the traction-separation law.
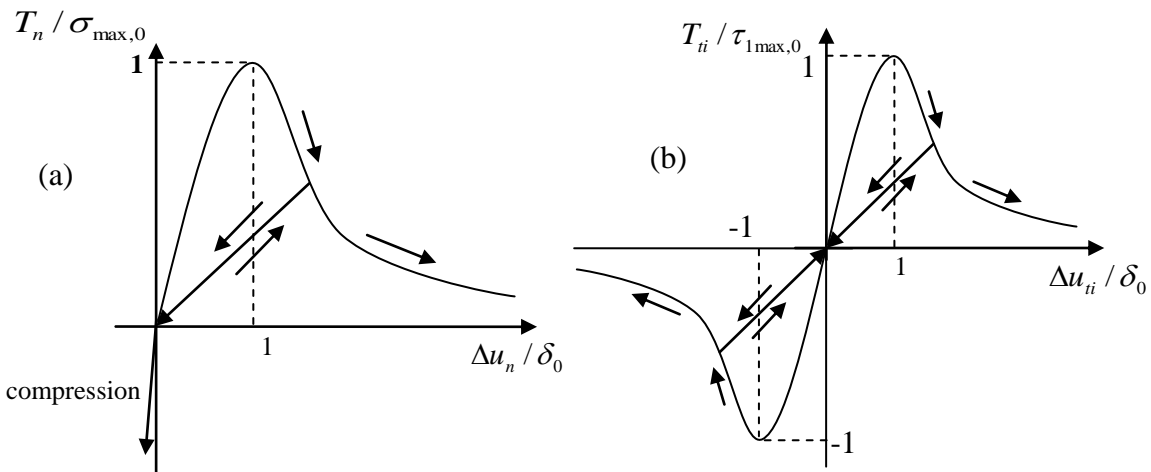

Figure 2.   Unloading/reloading paths for (a) pure normal and (b) Pure shear (i=1for tangential; i=2 for transverse).

3.   FINITE ELEMENT IMPLEMENTATION AND FRACTURE ANALYSIS

The cohesive zone model can be implemented into finite element analysis as mixed boundary conditions or incorporated in the form of cohesive elements. Here, we use cohesive elements to describe the nonlinear fracture process of materials.

The Finite Element software package ABAQUS [1] offers a library of cohesive elements and separation behavior of the cohesive elements can be well defined within the specific constitutive relations. In this section, the exponential cohesive zone model presented earlier is implemented through a user defined subroutine UMAT. The cohesive element type COH3D8 is made use of for the three-dimensional finite element models. The cohesive element has 8 nodes and 4 integration points (Figure 3)**.** The surface defined by nodes 1-2-3-4 and the surface defined by nodes 5-6-7-8 constitute the two virtual surfaces for purpose of crack propagation. Under the influence of the applied load, the two surfaces of the cohesive elements separate from each other and the relationship between traction load and separation follows the defined constitutive law.
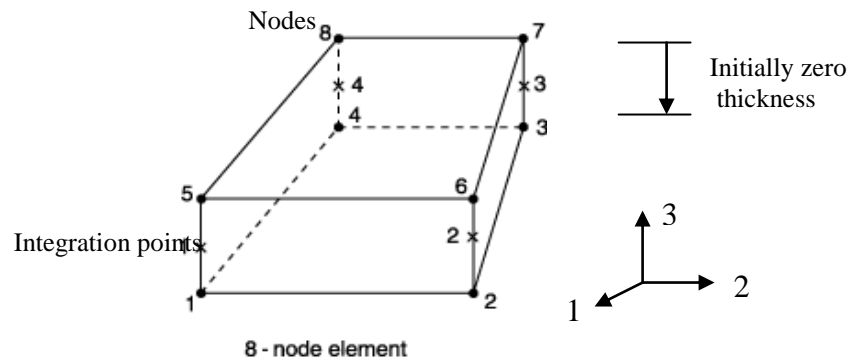
Figure 3.   **The COH3D8 cohesive element**.

3.1 Finite element implementation and verification

To first verify the numerical cohesive zone model implemented in the UMAT, a three-element finite element model is generated, which consists of two volumetric solid elements and one cohesive element having an initially zero thickness sandwiched in between, as shown in Figure 4 (a). The boundary conditon of the model is defined by restraining the three degrees of freedom (DOFs) at the bottom surface. A couple of cycles of normal loading with R=-1 is applied at the top surface nodes, in a manner that the cohesive element is loaded, unloaded and compressed prior to being reloaded and completely broken.

In Figure 4 (b) is shown the normal traction-separation curve of the cohesive element under conditions of monotonic loading and its response under both contact and compression. An exponential form is displayed for the monotonic loading unloading/reloading. Assuming $\tau_{i\max,0} = \sigma_{\max,0}$ ($q = 1/\sqrt{2e} \approx 0.4289$), the cohesive element presents similar exponential relations with a monotonic shear/transverse loading as shown in Figure 2, while a negative shear separation occurs during reversed shear loading/unloading.

The adopted form of the traction-separation model tends to reduce the traction value exponentially to zero with increasing separation. In an attempt to provide a consistent definition for the amount of crack extension, the advancing crack tip is defined at $\Delta u_n = 5\delta_0$ or $\Delta u_{ti} = 3\delta_0$ ($i = 1$ for tangential and $i = 2$ for transverse). The element is considered to be broken at the current integration point when the critical separation is reached, and consequently a new crack tip is defined at this point.
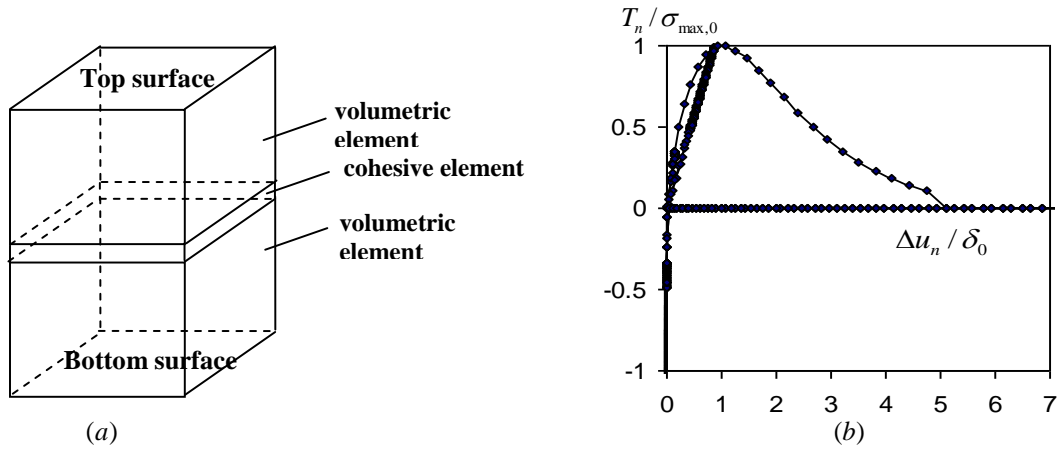
Figure 4. **(a)** **A three-element model containing two soild elements and one cohesive element.**
(b) **Normal traction-separation relation with contact behavior**.

3.2 Application in fracture analysis

To apply the verified cohesive model for fracture analysis, a high constraint Compact-Tension (CT) specimen and a low constraint Middle-cracked Tension (MT) specimen made from a thin sheet of aluminum alloy 2024 were modeled. For the purpose of predicting fracture behavior of the cracked specimens, cohesive elements having an initially zero thickness were defined along the potential crack path. The cohesive parameters were calibrated in a phenomenological way by fitting the numerical outcome with experimental data. Constant values were chosen and used for the computational efficiency and the validity was evaluated for different specimen types and geometries.

The geometry of the specimens tested is shown in Figure 5. The CT specimen has a width dimension of 150mm while the MT specimens have a dimension of 2W = 300 mm and crack length ratios of a/W = 0.33, a/W = 0.4 and a/W = 0.56. All of the specimens have a uniform thickness of 2.3mm. The material chosen for this study was aluminum alloy 2024-T3. In the longitudinal (*L*) orientation, the sheet material has a yield stress of 345 MPa, Young's Modulus of 71.3 GPa, and a Poisson's ratio of 0.3. The stress - strain curve for the chosen material is shown in Figure 6. The elastic-plastic property of the material enables possibility of plastic deformation of the bulk material during the quasi-static fracture process.

Crack front tunneling was observed in the crack extension experiments of specimens having finite thickness, where an initially straight crack front usually grows to become a curved shape. This phenomenon results from the conjoint influence of complex crack tip stress state, and conditions of external constraint. The interior, near plane-strain stress state enables faster growth of the crack compared to the state of plane-stress at the outer surface. In the three-dimensional cohesive zone model (CZM) simulation of the compact tension (CT) and middle tension (MT) specimens, the tunneling effect is revealed even for thin sheets of the chosen aluminum alloy.
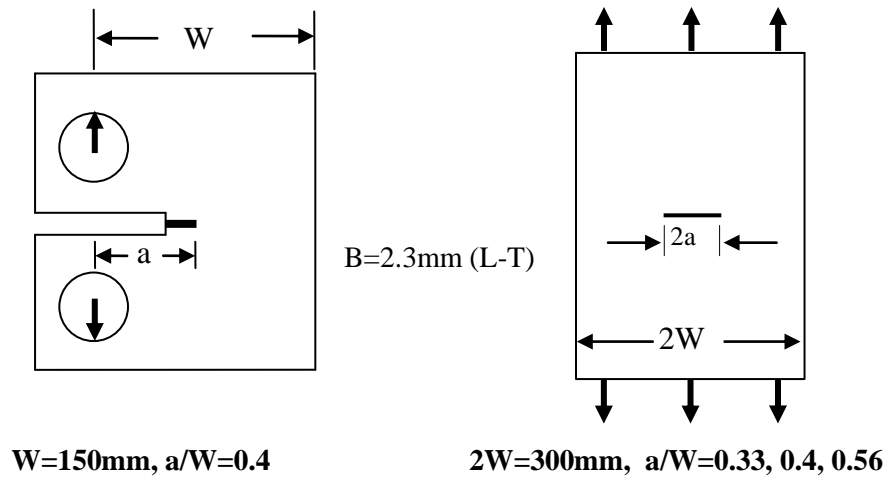
W=150mm, a/W=0.4   **2W=300mm, a/W=0.33, 0.4, 0.56**

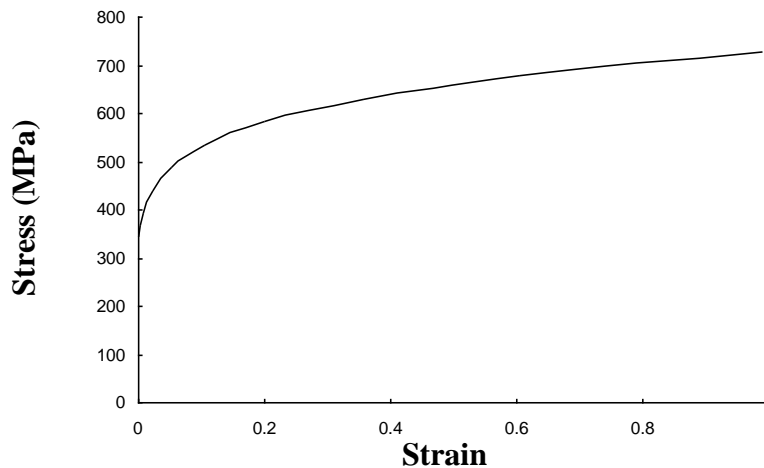**Figure 5.**   **Representative geometry of the specimens.**

Figure 6.   **True stress-strain curve of aluminum alloy 2024-T3 (longitudinal orientation)**

3.2.1 Modeling the CT specimen and Calibration of the Cohesive Parameters

To adequately resolve both the stress and strain fields in the cohesive zone at the crack tip, the finite element model should bear sufficient refinement of the mesh. Also, large-size elements may fail to capture the peak of the traction-separation curve resulting in inaccuracy and numerical instability. The length of the cohesive zone model introduced a characteristic length scale as reference. According to Roy and Dodds, 2001 [26], an element size of no more than 50 times the cohesive length generates numerically stable solutions when the values of the peak cohesive stress is less than three times the yield stress. They used a cohesive element size of 0.25 mm along the direction of crack advance, which is consistent with Siegmund and Brocks, 2000 [31], and obtained good results using a research code WARP3D for the same 2024 aluminum alloy. In the thickness direction, it was shown that four layers of finite elements were able to capture the through-thickness gradients of field quantities and the tunneling phenomenon in the immediate vicinity of the crack front.

Here fracture specimens of the thin 2024 aluminum alloy panels are analyzed using ABAQUS [1] with the cohesive zone model defined by the UMAT described previously. The in-plane size of the cohesive element is 0.1mm. Due to symmetry only half thickness is considered. Four layers of the solid (C3D8R) and cohesive (COH3D8) elements over the half-thickness direction were modeled for all the specimens. As shown in Figure 7, the finite element models tended to minimize mesh dependencies on crack growth response for the chosen mesh consideration. A typical model for the C(T) specimen contains 43,000 solid elements and 1,780 cohesive elements.

Parameters of the cohesive zone model are calibrated by matching the predicted tensile load *versus* crack extension with the experimental results obtained for the C(T) specimen. A series of calibration analyses for the C(T) specimen provide the needful parameters for the traction-separation model.
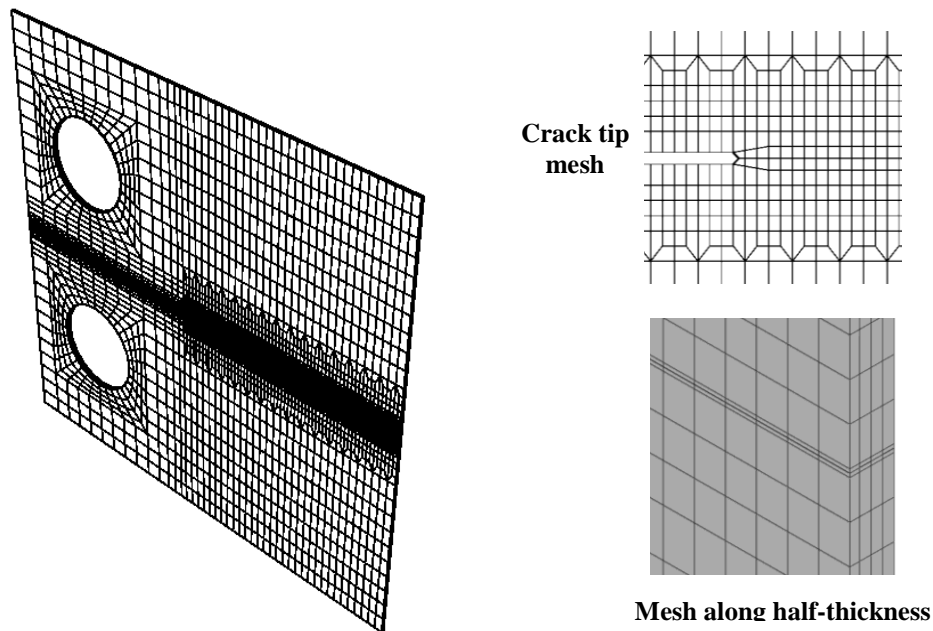
Crack tip mesh

Mesh along half-thickness

Figure 7.   The Finite Element model for the compact tension (CT) test specimen

In Figure 8 is depicted the effect of changes in the value of cohesive strength. For a constant value of the cohesive energy, a higher cohesive strength yields a higher external load while a lower cohesive strength yields a lower value of the external load. With a 5% change in the value of cohesive strength, the maximum external load is changed by about 14%. The force required for crack initiation remained almost the same for the same cohesive energy. The simulated results are summarized in Table 1.

By comparison, the change in cohesive energy causes less variance in the external load. For a constant value of the cohesive energy, a 10% change in the cohesive energy value resulted in less than 3% change in the computed external force. This is well represented in Figure 9. The simulated results are summarized in Table 2. Thus, it is concluded that the influence of cohesive strength is greater for this particular case when compared to cohesive energy.
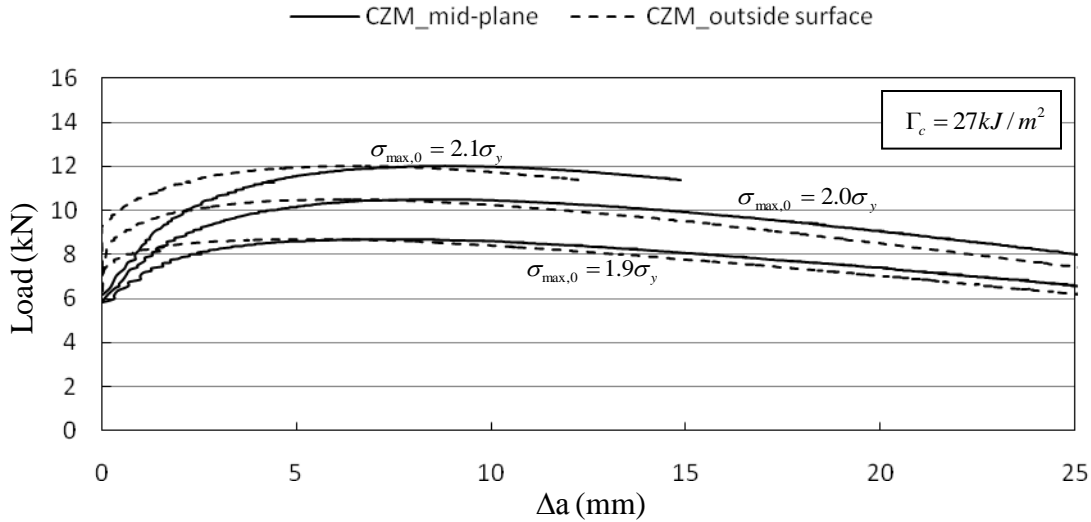
Figure 8. **The effect of cohesive strength on the predicted load versus crack extension response.**

Table 1: Effect of cohesive strength

Cohesive strength $\sigma_{max,0}$	Peak external load (kN)
$1.9\sigma_y$	**9.1**
$2.0\sigma_y$	**10.5**
$2.1\sigma_y$	**12.0**

Table 2: Effect of cohesive Energy

Cohesive energy $\Gamma_c (kJ/m^2)$	Peak external load (kN)
29.7	**10.71**
27.0	**10.48**
24.5	**10.12**

By comparing the numerical results with the experimental data, a group of cohesive parameters that result in a best agreement between the numerical and experimental results are listed as follows

$$\sigma_{max,0} = 2.0\sigma_y = 690\,MPa,\ \delta_0 = 0.0144\,mm,\ \Gamma_c = 27kJ/m^2.$$

These results are consistent with those obtained and recorded by Roy and Dodds, 2001 [26]. In Figure 10 is presented the results of the calibrated cohesive zone model and compared with the experimental data. The mid-plane crack propagation accorded well with the experimental results. The outside crack simulation appeared rigid in the beginning, although an initiation load of 7.0 kN and a peak load of 10.485 kN accord well with the experimentally obtained values.

The crack plane profile ahead of the initial crack front after a certain amount of crack extension is shown in Figure 11(a). Strong crack-front tunneling for the thin compact tension (CT) specimen reveals that the crack growth started at the mid plane, and crack extension gradually decreased from the mid-plane to the outside surface.

In Figure 11(b) is shown crack tunneling with respect to propagation length and compared with the experimental test results obtained by Dawicke and Sutton, 1994 [5]. For the Longitudinal-Transverse (L-T) orientation of aluminum alloy (2024-T3) sheet, the crack front transformed into a visible 'shear' mode of ductile tearing following crack propagation for a short length along the center plane. However, in the numerical model the cohesive elements are placed

along the center plane and crack propagation is restricted to the 'flat' mode. The simulated tunneling does not represent the complete tunneling behavior but is effective only for the early stages of crack propagation.
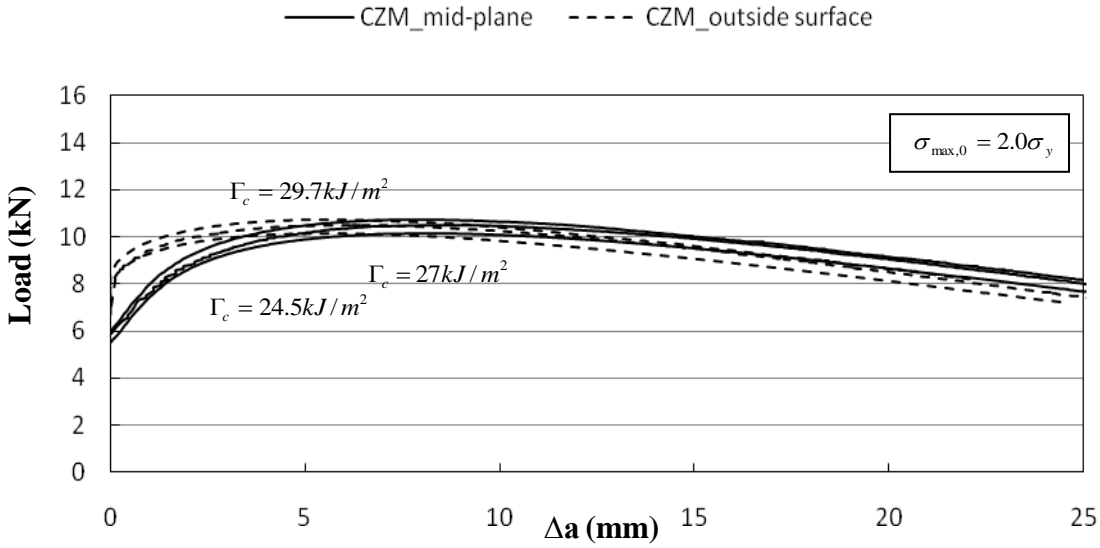

Figure 9.   **The effect of the cohesive energy on predicted load vs. crack extension response.**
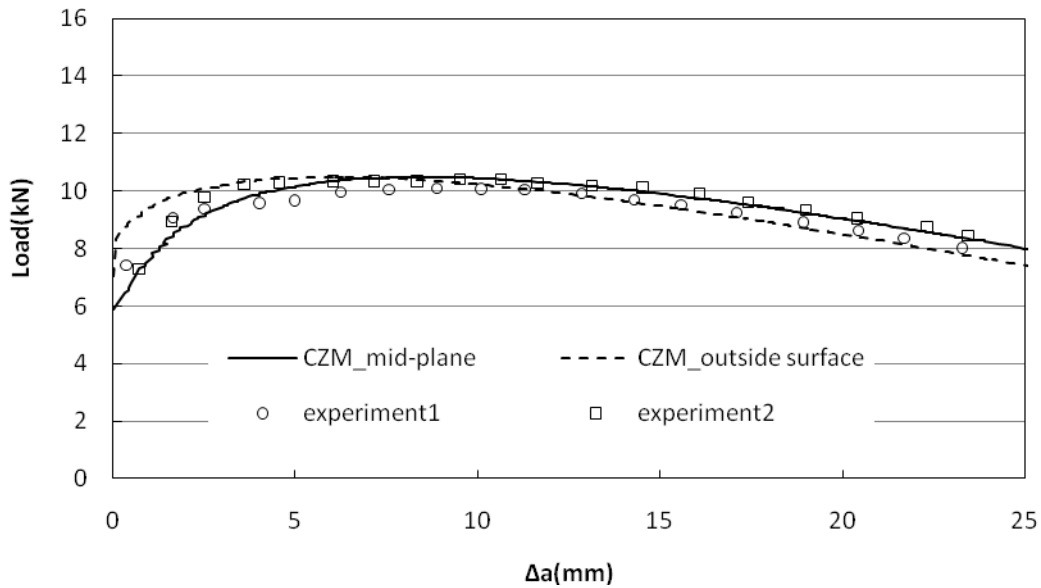

Figure 10.   **Cohesive zone model (CZM) simulation results of the compact tension (CT) test specimen compared with the experiments**
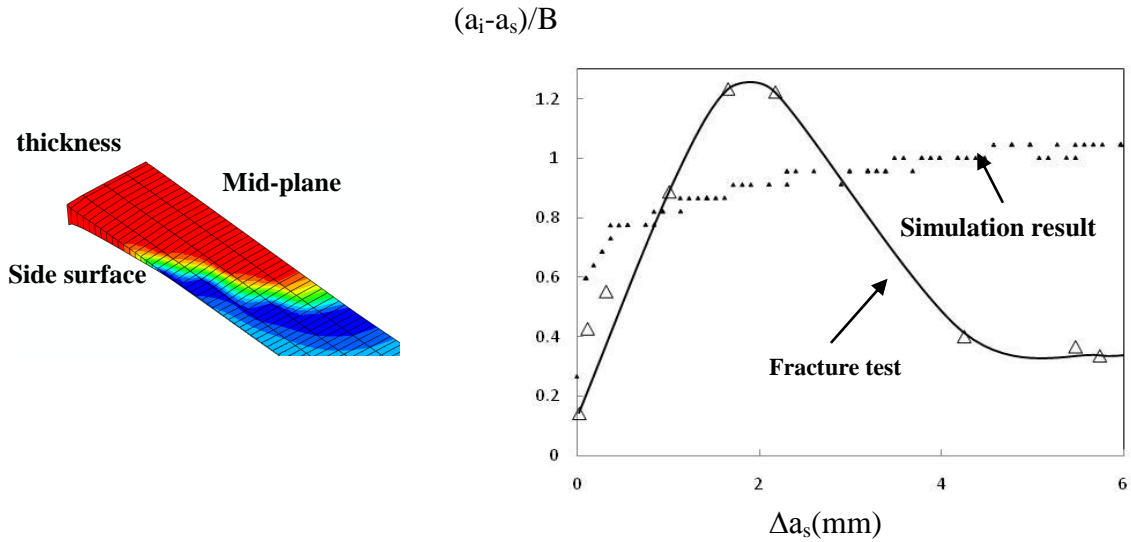
$(a_i-a_s)/B$

Δa_s(mm)

Figure 11. **(a)**   **Profile of the crack surface;**
(b)   **Tunneling effect compared with fracture test,**
where a_i represents the crack length at the mid-plane and a_s represents the crack length at the side surface.

3.2.2 Cohesive zone modeling for the MT specimens

The Middle-cracked Tension (MT) specimens having a dimension of 2W=300mm, and crack length to specimen width ratios of a/W = 0.33, a/W = 0.4 and a/W = 0.56 have been modeled using the same cohesive parameters that were calibrated from simulation results on the CT specimen. Symmetry was applied so that one fourth of the specimen is modeled. The same mesh refinement is adopted here, i.e., the size of the cohesive element is 0.1 along the crack path direction and four layers of elements are placed in the thickness direction over half thickness of the specimen. In Figure 12 is shown a typical mesh. The cohesive zone was properly resolved with such considerations for the mesh, thereby avoiding dependency on the mesh. A typical MT model for crack growth simulation contained 47,000 solid elements and 1,984 cohesive elements.
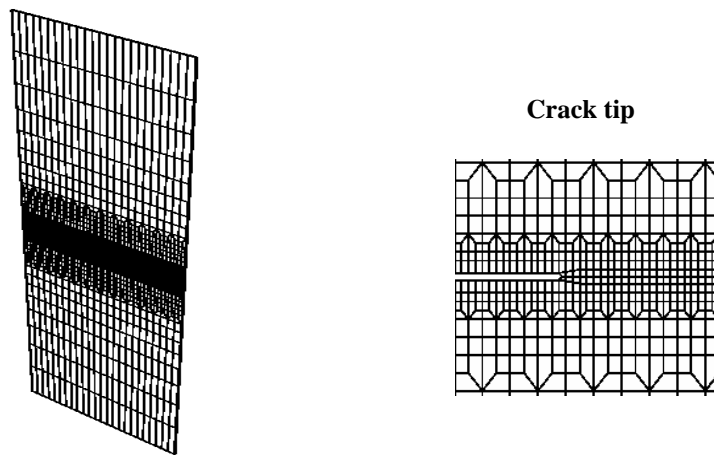

Figure 12.   **Finite Element model of the Middle Tension (MT) specimen**

Results of the numerical simulation are shown in Figure 13. The curves plotted are for crack extension on the outside surface of the specimen. Experiments for different ratios of the crack length are also shown for purpose of comparison. Using the same cohesive parameters that were calibrated from the results of simulation of the C(T) specimen, the MT simulation fits well with the experimental results. Larger ratios of the crack length correspond to an overall higher value for the curve, i.e. a lower remote stress is needed for both crack initiation and subsequent crack propagation for the case of the longer cracks.
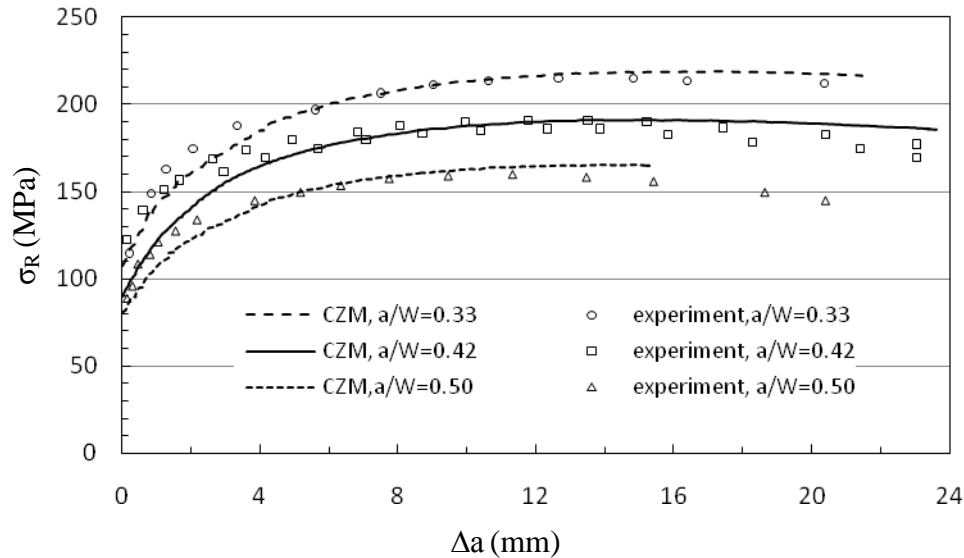

Figure 13. **CZM simulation results of MT specimens compared with the experiments**

It is to be noted that the finite element simulations were at times terminated due to convergence issues after the cracks had propagated to a certain length. The numerical considerations concerning convergence and related to non-linear material behavior will be addressed in a companion paper (Haodan and co-workers, 2010 [12]) and evidently reveal improved computational capacity.

4.   DISCUSSIONS AND FUTURE CONSIDERATIONS

A cohesive zone model with an exponential traction-separation law was implemented in a finite element software ABAQUS via a user defined subroutine for simulation of crack growth under monotonic loading. The cohesive zone model is governed by two key parameters: (i) the cohesive energy, and (ii) the cohesive strength. Parameter study suggests the influence of the cohesive strength is much stronger. The cohesive zone model is applied to simulate crack propagation in specimens made from thin 2024 aluminum panels. The cohesive parameters are calibrated using the C(T) specimen and then used to predict crack growth in the MT specimens. The cohesive zone model (CZM) simulation results accord well with the experiments by capturing the essential crack growth behavior from initiation throughout the process of propagation.

Numerical applications proved the cohesive zone model to be an effective tool for crack growth study under conditions of monotonic loading. For crack growth under cyclic loading, degradation of the material needs to be taken into account. A companion technical manuscript (Jiang, Gao and Srivatsan, 2010 [12]) presents and discusses an irreversible cohesive zone model and crack growth under the different modes of loading.

Future work needs to look further into numerical problems and careful considerations must be provided for the individual modeling case, especially for three-dimensional simulations where the burden of computation increases significantly. The influence of local constraint, mixed-mode loading, and normal/shear coupling also deserve continued investigation.

REFERENCES

[1] ABAQUS, ABAQUS reference manuals (v6.7). 2007. Providence, RI.

[2] Barrenblatt G.I. (1962) The mathematical theory of equilibrium of cracks in brittle Fracture. *Advances in Applied Mechanics.* 7, 55–129.

[3] Bouvarda J.L. and Chabocheb J.L. (2009) A Cohesive Zone Model for Fatigue   and Creep-Fatigue Crack Growth in Single Crystal Superalloys. *International   Journal   of Fatigue*. 31(5), 868-879.

[4] Camacho G. and Ortiz M. (1996) Computational modeling of impact damage in brittle materials. *International Journal of Solids and Structures*. 33, 2899–2938.

[5] Dawicke D.S. and Sutton M.A.. (1994) CTOA and Crack-Tunneling Measurements in ThinSheet 2024-T3 Aluminum Alloy. *Experimental Mechanics*. December: 357-368.

[6] Dowling N. and Begley J. (1976) in: Mechanics of Crack Growth, ASTM STP 590, American Society for Testing and Materials, Philadelphia, PA, pp. 83–104.

[7] Dugdale D.S. (1960) Yielding of steel sheets containing slits. *Journal of the Mechanics and Physics of Solids.* 8, 100–104.

[8] Foreman R., Keary V. and Engle R. (1967) Numeral analysis of crack propagation in cyclic loaded structures. *Journal of Basic Engineering.* 89, 459–464.

[9] Foulk J.W. and Allen D.H. (2000) Formulation of A Three-Dimensional Cohesive Zone Model for Application to A Finite Element Algorithm. *Computer Methods in Applied Mechanics and Engineering*. 183, 51-66.

[10] Irwin G.R. (1956) Onset of Fatigue Crack Propagation in High Strength Steel   and Aluminum Alloys, *Sagamore Research Conference Proceedings*, Vol. 2, pp. 289-5305.

[11] Jiang H., Gao X. and Srivatsan T.S. (2009) Predicting the influence of overload and loading mode on fatigue crack growth: A numerical approach using irreversible cohesive elements. *Finite Elements in Analysis and Design.* 45, 675-685.

[12] Jiang H., Gao X. and Srivatsan T.S. (2010), A Cohesive Zone Model for   Studying Crack Growth in Materials Under the Influence of Cyclic Loading, submitted for publication.

[13] Lemaitre J. (1996) A Course on Damage Mechanics. Springer, Berlin.

[14] Lemaitre J, and Chaboche, J. Mechanics of Solid Materials, Cambridge University Press, Cambridge, 1994.

[15] Levy A.J. (1994) Separation at a Circular Interface under Bi-Axial Loading. *Journal of the Mechanics and Physics of Solids.* 42, 1087–1104.

[16] Li W. and Siegmund T. (2002) An analysis of crack growth in thin sheet metal via a cohesive zone model. *Engineering Fracture Mechanics.* 69, 2073–2093.

[17] Lin G. and Cornec A. (1998) Three-Dimensional Finite Element Simulation of Crack Extension in Aluminum Alloy 2024. *Fatigue & Fracture of Engineering Materials & Structures.* 21, 1159-1173.

[18] Miller O., Freund L.B. and Needleman A. (1999) Modeling and Simulation of Dynamic Fragmentation in Brittle Materials. *International Journal of Fracture*. 96, 101–125.

[19] Needleman A. (1992) Micromechanical modeling of interfacial decohesion. *Ultramicroscopy.* 40, 203–214.

[20] Nguyen O., Repetto E.A., Ortiz M. and Radovitzky R.A. (2001) A cohesive model of fatigue crack growth. *International Journal of Fracture.* 110, 351–369.

[21] Ortiz M. and Pandolfi A. (1999) Finite-deformation irreversible cohesive elements for three-dimensional crack propagation analysis. *International Journal for Numerical Methods in Engineering.* 44, 1267–1282.

[22] Pandolfi A., Guduru P.R. (2000) Three Dimensional Cohesive-Element Analysis and Experiments of Dynamic Fracture in C300 Steel. *International Journal of Solids and Structures.* 37, 3733-3760.

[23] Paris P. and Erdogan F.A. (1963) Critical analysis of crack propagation laws. *Journal of Basic Engineering.* 85, 528–534.

[24] Repetto E.A., Radovitzky R. and Ortiz M. (2000) Finite element simulation of dynamic fracture and fragmentation of glass rods. *Computer Methods in Applied Mechanics and Engineering.* 183, 3-14.

[25] Rice J.R. (1968) Mathematical analysis in the mechanics of fracture, in: H. Liebowitz (Editor), *Fracture-An Advanced Treaties.* vol. 2, Academic Press, New York, London, pp. 191–311.

[26] Roy Y. A. and Dodds R.H. (2001) Simulation of ductile crack growth in thin aluminum panels using 3-D surface cohesive elements. *International   Journal of Fracture,* 110, 21–45.

[27] Roychowdhury S., Roy Y.A. and Dodds R.H. (2002) Ductile tearing in thin aluminum panels: experiments and analyses using large-displacement, 3-D surface cohesive elements. *Engineering Fracture Mechanics.* 69, 983–1002.

[28] Scheider I. (2001) Simulation of Cup–Cone Fracture in Round Bars Using the Cohesive Zone Model. In: Bathe K-J, (Editor). *First MIT Conference on Computational Fluid and Solid Mechanics.* Elsevier, pp. 460–462.

[29] Scheider I. and Brocks W. (2003) Simulation of Cup–Cone Fracture Using the Cohesive Model. *Engineering Fracture Mechanics.* 70, 1943–1961.

[30] Siegmund, T. and Needleman, A. (1997) A numerical study of dynamic crack growth in elastic-viscoplastic solids. *International Journal of Solids and Structures.* 34, 769-788

[31] Siegmund T. and Brocks W. (2000) A Numerical Study on the Correlation Between the Work of Separation and the Dissipation Rate in Ductile Fracture. *Engineering Fracture Mechanics.* 67, 139-154.

[32] Suo Z., Ortiz M. and Needleman A. (1992) Stability of Solids with Interfaces. *Journal of the Mechanics and Physics of Solids*, 40, 613–640.

[33] Willenborg J., Engle R. and Wood R. (1971) Technical Report AFFDL-TM-71-1 FBR. Air Force Flight Dynamics Laboratory.

[34] Wheeler O. (1972) Spectrum loading and crack growth. *Journal of Basic Engineering* 94, 181–186.

[35] Xu X. and Needleman A. (1994) Numerical simulations of fast crack growth in brittle Solids. *Journal of the Mechanics and Physics of Solids.* 42, 1397–1434.

[36] Zhai J. and Zhou M. (2000) Finite Element Analysis of Micromechanical Failure Mode in Heterogeneous Brittle Solids. *International Journal of Fracture*, 101, 161–180.